Bioprinting 20 (2020) e00090

Contents lists available at ScienceDirect

Bioprinting

journal homepage: www.elsevier.com/locate/bprint

3D printing and bioprinting using multiphoton lithography

Dmitry M. Zuev [a], Alexander K. Nguyen [b], Valery I. Putlyaev [a], Roger J. Narayan [b,*]

[a] Department of Materials Science, Lomonosov Moscow State University, Russia
[b] Department of Biomedical Engineering, North Carolina State University, United States

ARTICLE INFO

Keywords:
3D printing
Multiphoton lithography
Tissue engineering scaffold
Cytotoxicity
Biocompatibility

ABSTRACT

3D printing based on multiphoton absorption is playing a growing role in biomedical engineering and regenerative medicine. Multiphoton lithography is a 3D printing approach that is based on the multiphoton absorption process. The review focuses on the use of multiphoton lithography to create microneedles, microfluidic devices, nanoprobes, filters, and tissue engineering scaffolds with sub-micrometer scale features. The fundamental requirements of the multiphoton absorption process are described. Efforts to increase the processing rate as well as understand the bioresorbability of multiphoton lithography-created structures are discussed. Improvements to the biocompatibility of the polymers and photoinitiators used in multiphoton lithography are considered. The multiphoton lithography process offers unique opportunities to process tissue engineering scaffolds with small-scale features.

1. Introduction

The multiphoton absorption process was first described by Maria Goeppert-Mayer in 1931 [1]. Multiphoton lithography is a 3D printing process that uses multiphoton absorption for selective solidification of a photosensitive resin and 3D printing of objects with fine-scale (e.g., sub-micrometer) features. It has been used to prepare structures with small-scale features for a variety of technological applications [2] such as photonic crystals [3] and optical data storage devices [4–6]. This approach [7] is particularly useful for creating microscale devices, including monolithic valves, pumps, and probes [7–13].

Multiphoton lithography has played a significant role in preparing structures with small-scale features for biomedical applications, including biomimetic structures [14] and scaffolds for tissue engineering [15–18]. The use of multiphoton lithography for biomedical applications is an emerging field that encompasses medicine, optics, and materials science.

The use of multiphoton lithography is associated with several significant challenges [19]. The materials (e.g., composites [20,21], organic-inorganic polymers [22], and photoresists [23]) must be transparent to infrared light. The slow speed of multiphoton lithography limits the use of this approach [24]. The low scanning rate for multiphoton lithography makes it difficult to create macroscale structures with high-resolution features [25]. Efforts have been made to enhance the processing speed through the use of a Q-switched microchip laser [26]. Scaffolds for tissue engineering and other structures for biomedical applications should exhibit biocompatibility; for some applications, the ability to be resorbed by the body is also desirable [27]. Most of the photoinitiators in use today are toxic; some biocompatible photoinitiators such as the mixture of riboflavin and triethanolamine have been developed [28]. Fig. 1 shows optical images of 50% polyethylene glycol diacrylate scaffolds, which were polymerized with a riboflavin–triethanolamine mixture, in water. However, the riboflavin–triethanolamine mixture is less efficient than conventional photoinitiators (e.g., Irgacure® photoinitiators). Overcoming these limitations can lead to a significant increase in the use of multiphoton lithography for 3D printing and bioprinting.

2. The working principle of multiphoton lithography

As mentioned above, multiphoton lithography is based on the multiphoton absorption process; the probability of linear photon absorption process in the focal volume is proportional to the power function of intensity [29,30]; it is proportional to the square of intensity for the two-photon process [31] and the third power for three-photon absorption. The extended for multiphoton absorption version of Beer's law is shown below:

$$\frac{\partial I}{\partial z} = -\left(\alpha_1 I + \alpha_2 I^2 + \alpha_3 I^3 + \ldots\right)$$

* Corresponding author. Joint Department of Biomedical Engineering, University of North Carolina and North Carolina State University, Raleigh, NC, USA.
E-mail address: roger_narayan@unc.edu (R.J. Narayan).

https://doi.org/10.1016/j.bprint.2020.e00090
Received 8 May 2020; Received in revised form 14 July 2020; Accepted 15 July 2020
2405-8866/© 2020 Elsevier B.V. All rights reserved.

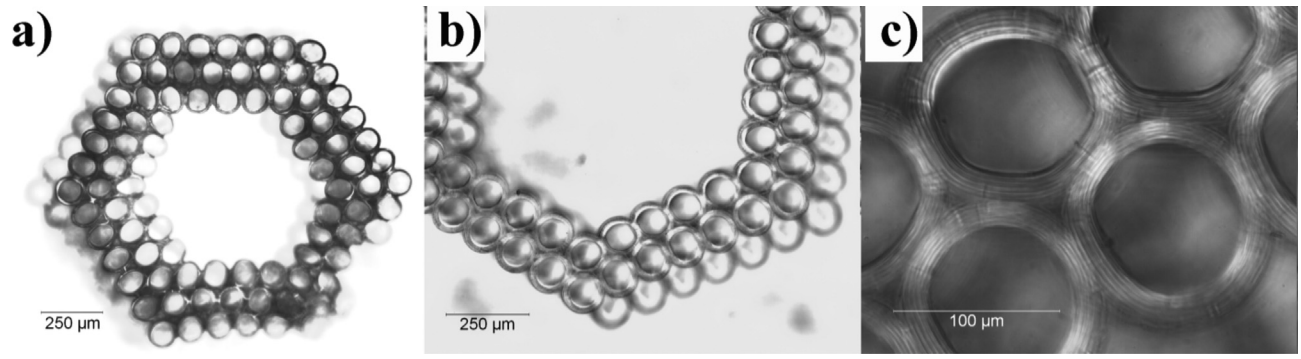

Fig. 1. Optical images of 50% polyethylene glycol diacrylate scaffolds polymerized with a riboflavin–triethanolamine mixture in water. Reproduced with permission from Ref. [28].

In this equation, δz is a longitude of the focal voxel, α_1 is the linear absorption coefficient, α_2 is the two-photon absorption coefficient, and α_3 is the three-photon absorption coefficient. The SI units of the coefficients are m/W [30]. The two-photon absorption coefficient is defined by the following equation:

$$\alpha_2 = \frac{2\hbar\omega}{I^2}\nu_{2PA} = \frac{N}{E}\sigma_{2PA}$$

In this equation, ħ is the Dirac constant, ω is the laser frequency, I is the irradiance or power (radiant flux) per focused volume, ν is the transition rate of two photon absorption (2PA) per voxel, N is the density of the photoresist (the number of reaction molecules in the voxel), E is the photon energy, σ is the 2PA cross-section in cm^4 s per photon. The equation is presented for the 2PA case [32].

Due to Heisenberg's uncertainty principle, increasing the laser frequency generates spectrally stretched signal or bandwidth-limited pulses. A laser pulse compressor is used to generate pulses with sufficient power for reaching the objective and producing 2PA; the frequency can be determined by an autocorrelator. 2PA is possible with femtosecond lasers, which have low average power and very high peak power values.

The multiphoton lithography approach may include a chirped (or axially dispersed) pulse amplification (CPA) system [33]. A diffraction grating can spectrally and simultaneously stretch the pulse via angular dispersion. It leads to a reduction in peak power that is incompatible with 2PA.

High-resolution MEMS devices can be obtained using this approach [34–37]. To get a clear beam without undesirable low power areas, a pinhole spatial filter can be used. The pinhole spatial filter allows only the low spatial frequencies to pass to the objective [38].

One of the fundamental requirements for multiphoton lithography is femtosecond lasers and a high laser intensity [39,40]. Pulses from a nonamplified femtosecond laser (50–150 fs, 10–100 kHz, 10–700 mW [41]) can induce two-photon photopolymerization and produce devices with sub-micrometer features such as photonic crystals [42].

A photoinitiator (PI) is required for multiphoton polymerization via multiphoton absorption [43]. On exposure to light, a PI produces photoradicals, which interact with monomers in the photoresin to (a) catalyze photopolymerization or polycondensation of a negative photoresist, making an insoluble cross-linked network, and (b) catalyze photodegradation in case of positive photoresists. Postcuring by developers can lead (a) to mostly dissolving the uncured area for a negative photoresist or (b) mostly dissolving the cured areas for positive photoresist. The quality of the photoresist is characterized by the quantum yield (QE). QE can be defined as the ratio of the number of converted photoinitiators to the number of photons absorbed by the initiators [44]. Converted photoinitiators are the radicals in T_1 state after intersystem crossing from the excited S_1 state. There are a number of commonly used photoinitiators for initiating 2PA; these include Irgacure® 184, 651, 819, 261, 369, 907, 754; OXE-01; CD-1012/ITX,; Darocure® TPO; and SpeedCure MBF [45].

The QE of the photoinitiator or the energy conversion efficiency can be enhanced by fluoride-based inorganic upconverting nanoparticles [46], covalently-bonded photosensitizers with chromophores [40], or centrosymmetric chromophores, which are preferable due to the absence of transition of one photon absorption (1PA) from the ground state to the excited state (Fig. 2 I) [47,48].

In the case of 2PA, the generation of the second harmonic occurs through a simultaneous resonant interaction of photons with $E_{1,2} = 2{\cdot}h\nu_{1,2}$ in a virtual state that is distinct from one-photon absorption ($E_3 = h\nu_3$ + excited-state absorption, or ESA) to reach the S_n state. The excited system undergoes internal conversion (IC) or non-radiative transitions in the process of relaxation. Fluorescence is accompanied by the presence of internal conversion from S_1 to S_0 and by intersystem crossing (ISC) to a triplet state T_1 (Fig. 2 II) [47]. Triplet relaxation (phosphorescence) has slower relaxation time (10^5 - 10^{-3} s^{-1}) and is more stable in comparison with fluorescence (10^{10}–10^7 s^{-1}) [49]. Therefore, the 2PA is based on a transition from the triplet state to the ground state. Due to its sufficient intensity and relatively stable condition, T_1 undergoes ISC and transfers energy to the PI in order to induce a photoreaction.

Ultra-fast lasers can produce features below the diffraction limit by regulation of the quantity and energy of laser impulses [50]. The polymerization process, which is initiated by exposure to high-intensity laser energy, theoretically occurs inside a reaction threshold area, which has a Gaussian-like form. The transition from one-photon to two-, three-, and greater photon absorption can decrease the threshold for the polymerization area or voxel [51]. The focal point generated by multiphoton polymerization may be larger than the diffraction limit as observed in the Airy disk; however, the intensity of the light reduces the voxel size. The diameter of Airy disk is estimated as $d = 1.22{\cdot}\lambda/NA$, where λ is the wavelength of light, and NA is the numerical aperture of the objective lens. For example, $d = 1.22{\cdot}(780/2)$ nm$/1.4 = 340$ nm is the minimal theoretical volume of the voxel for a 780 nm excitation wavelength in 2PA; however, 2PA occurs only in the area inside this disk where intensity is sufficient. As such, structures smaller than this volume can be processed [3]. The smallest resolution of 2PA is in the sub-50 nm region [52]. Single-photon absorption has an Airy disk of ~340 nm at an excitation wavelength of 380 nm. The real voxel for 2PA is less than estimated Airy disk; the requirement of sufficient intensity for 2PA results in absorption only inside the zero ring area of the Airy disk [53]. Since multiphoton lithography is not a diffraction-limited process, Rayleigh, Abbe, or Sparrow separation criteria do not apply. A square grid of diffraction-limited dots was obtained with a spatial light modulator (SLM) refresh [54]. The d_z/d_{xy} ratio in a voxel can be reduced up to 1.5–3 by using objectives with a high NA (~1.4) [55]. In addition, axial resolution can be gained through the use of shaded-ring filters [39]. The axial length of the voxel was reduced from 1.43 μm to 1.13 μm while a lateral length of 0.99 μm was retained; as such, the eccentricity was reduced by 33% [56].

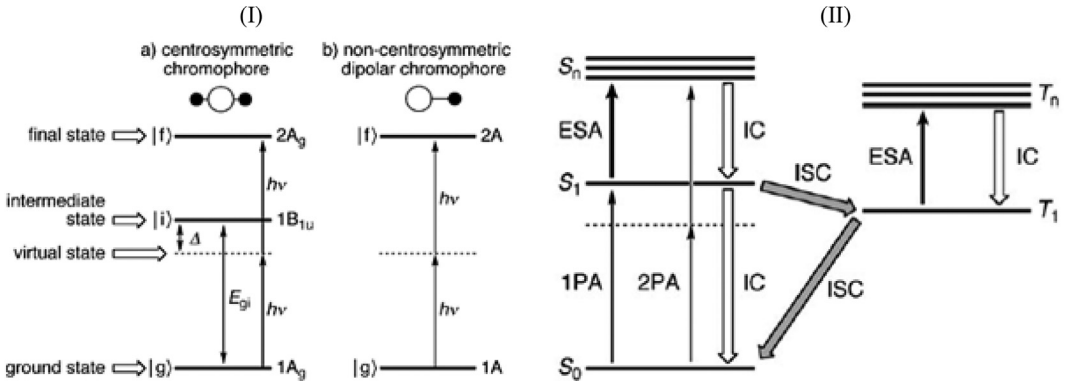

Fig. 2. (I) Energy level diagrams for the essential states in a) centrosymmetric and b) non-centrosymmetric chromophores. The diagram is the generic lowest 2PA transition in any centrosymmetric or noncentrosymmetric molecule. (II) Simplified Jablonski diagram for the optical power associated with 1PA or 2PA. Shown are the excited-state absorption (ESA), internal conversion (IC), and intersystem crossing (ISC). Reproduced with permission from Refs. [47].

3. Biomedical engineering applications of multiphoton fabrication

3.1. Biomedical microneedles

Microneedle arrays are small-scale devices that may be used for transdermal drug delivery in place of conventional syringe injections. Microneedles enable the delivery of drugs through the stratum cornum layer of the epidermis; these devices cause little or no pain and minimal skin trauma [57]. Microneedles may allow for intradermal delivery of vaccines with dose sparing since the dermis layer of the skin contains a high percentage of immune cells. Single microneedles or arrays of microneedles may be used for drug delivery [58]. Microneedles (h = 1 mm, d = 100 μm) mimicking the features of the mosquito proboscis were printed using multiphoton lithography. The needle consists of two independent parts, which replicate the central hollow labrum and two side maxillae, including jagged edges, of the mosquito proboscis. These two parts have a semi-circular channel and jagged edges for reducing the resistance force during the insertion process. The devices showed no mechanical deformations during insertion into artificial skin. Due to capillary force, this type of microneedle can take up blood for analysis [59]. Multiphoton lithography can also be used to fabricate arrays of microneedles [60].

3.2. Microfluidic devices

Multiphoton lithography has been used for processing several types of microfluidic devices [61]. A biomimetic device was prepared that contained a complex membrane (d = 2 mm) to replicate the nutrient transport features of the placental barrier; these types of membranes can be used to study fetal pathophysiology. The membrane was created using multiphoton lithography; it consisted of gelatin-methacryloyl-aminoethylmethacrylate (GelMOD-AEMA) and HUVEC cells [62]. The permeability of the membrane was studied in riboflavin and dextran solutions. Wall thickness, which is different during various stages of pregnancy, affects the distribution of dye and the scale of the transition zone. Dextran is located mostly outside the membrane. On the other hand, riboflavin is present both inside and outside the membrane; as such, the membrane exhibits selective transport properties.

3.3. Microfilters

Novel arch-like semi-channel cascade filters with enhanced efficiency were fabricated by two-photon fabrication since it is able to form structures with high precision and fine grid structures that are able to filter cells. A Y-shaped microchannel glass chip was obtained by chemical etching, then multi-focal fabrication and integration of the arch-like microsorter were followed [63]. A SLM [64] allows structures to be simultaneously processed in five foci processing areas to create (a) low-capture, (b) band-capture, and (c) high-capture sorters. Multimodal sorting was demonstrated using SiO_2 microparticles and SUM159 breast cancer cells from human blood [63].

3.4. Probes

Glassy carbon ultra-sharp tips were also prepared using multiphoton lithography [65]. This approach enabled AFM cantilevers to produced with a tip radius of 25 nm and a height of 30–100 μm [66]. Carbonization of the tips via pyrolysis shrinkage allowed structures with features lower than the diffraction limit to be produced [67]. These tips are capable of providing high-resolution AFM images from biological objects, including measurements of the mechanical properties of the cytoskeleton [68].

3.5. Scaffolds for tissue engineering

Scaffolds for tissue engineering must exhibit appropriate properties for direct contact with cells and tissues over an extended period of time. In a comparison with fused deposition modeling [69,70], stereolithography [71], or inkjet dispensing [72–74], 3D printing of porous scaffolds using multiphoton lithography faces several technical limitations. Osteoconductive honey-comb scaffolds were fabricated by multiphoton lithography; these scaffolds showed good biocompatibility and biomineralization [75,76]. Biomineralization is an important parameter for scaffolds used in bone tissue engineering [77–79]. Multiphoton lithography can be used to create sub-cellular features for understanding cell migration [80]. The mechanical properties of the structures can be enhanced by post ultraviolet light curing [81].

Multiphoton lithography can also be used to create channels for cell migration [82]. In addition, scaffolds can be created from hydrogels [83] for neural cell growth [84]. Scaffolds with sub-micrometer resolution containing gelatin methacrylate and fibronectin were used to create murine heart muscle scaffolds. The scaffolds were seeded by cells and were shown to enhance recovery after ischemic myocardial injury [85]. Multiphoton lithography can also be used for functional analysis of photo-stimulated activation of store-operated calcium (SOC) channels; exposure to a femtosecond laser energy has been shown to lead to a Ca^{2+} influx. The technique can be used to study signaling based changes in intracellular Ca^{2+} levels [86].

3.6. Imaging via two photon absorption

Two-photon laser fluorescence scanning microscopy is commonly used for high-resolution imaging of soft tissues [87–89]. Two-photon fluorescence microscopy of motor neurons and adjacent glia in the

ventral spinal cord [90], neuronal cell excitability [91], and ocular tissue [92] is possible due to deep penetration ability of near infrared light. A living tissue visualization in a depth of 1 mm can be obtained by multiphoton absorption with infrared light in contrast to the low penetration ability of ultraviolet or visible light [93]. However, high intensity absorption of infrared light at greater than 1400 nm by water must be taken into account [94]. Near infrared light is associated with less toxicity than one-photon imaging due to the absence of a number of endogenous absorbers in most living tissues [94].

A voxel with a constant radius shape in each direction can be obtained by 3D structured illumination microscopy (SIM) technology [95]. 2P-type SIM system is based on laser scanning microscopy [96]. A structured illumination technique can form a 3D signal by projecting a high resolution laser grid to a rough surface of biological objects via a Delaunay triangulation. As a result, structured illumination allows one to obtain doubling of physical NA, resulting in super-resolution microscopy [97]. It can get images from thick and scattered tissues up to 150 nm in the lateral orientation and 400 nm in the axial orientation [98]. This approach for multiphoton microscopy is limited since this approach uses a reconstruction of a number of images obtained using 2PA microscopy.

4. Technical challenges associated with multiphoton lithography fabrication of scaffolds for tissue engineering

Multiphoton lithography can produce structures with small-scale features at a slow processing rate [99,100]. Most scaffolds for tissue engineering are prepared at a higher processing rate than what is currently offered by multiphoton lithography [101]. Several technical limitations must be overcome for multiphoton lithography to play a greater role in scaffold processing.

4.1. Infrared (IR) absorbance by matter

The benefit of using an infrared laser for materials that are photosensitive to light in the ultraviolet or visible spectrum is that one can polymerize areas in the middle of the photopolymer using the dip-in approach (i.e., dipping the objective lens into the photoresist) [102]. This approach is of benefit since one cannot move the substrate (as in the stereolithography process) to obtain photopolymerization on the surface. Multiphoton absorption requires high photon density for simultaneous absorption and transition from the valence to the conduction band [103]. Decreasing the energy of the photons can lead to an increasing probability of absorption of laser energy by molecules that vibrate on infrared irradiation if three photon absorption (3PA) or higher are stimulated. Most currently available photopolymers are transparent in visible and near-IR range; this parameter limits the application of two-photon (or more than two photon) lithography [103].

High photon absorption and Willis–Tyndall scattering by inorganic particles and dyes occur in the near infrared spectrum [104]; as such, the photoresins must be transparent to near infrared spectrum. Scattering of liquid water in printed hydrogels in the 2PA process is less than in the 1PA process [105]. Two-photon 3D printing tries to overcome the problem of infrared absorption by using infrared transparent polymers [106], including materials on the Ormocer™ inorganic-organic hybrid material [50]. Femtosecond lasers with high frequency output avoid the formation of a heat-affected zone [51] and enable the voxel volume to be lowered.

One challenge is associated with the fabrication of composite structures for biomedical applications. Many photoresins used in multiphoton lithography are based on Ormocer™. The inorganic part consists of silicon alkoxides or alkoxysilane groups, which form an Si–O–Si network through hydrolysis and condensation. The (meth) acrylate undergo photochemical organic polymerization; covalent bonds form among the organic and inorganic components of the material [107]. It is used for the fabrication of microneedles [108] and free-standing scaffolds for tissue engineering. The appropriate cell proliferation properties of Ormocer™ were demonstrated using HT1080 epithelial-like cells and B35 neuroblast-like cells [109]. Ormocer™ provides an appropriate interface for cell growth [110]. The Fraunhofer Institute for Silicate Research developed a new BioOrmocer™ photoresin; it is produced by binding the basic Ormocer™ polymer with chitosan and the biodegradable polycaprolactone triol with zinc oxide, which provides the material with antimicrobial properties [111,112].

The Ormocer™ photoresin is a biocompatible material that is used for biomedical food, cosmetic, pharmaceutical applications [112,113]. 3D structures printed from the material exhibit appropriate mechanical properties [114] and cell proliferation properties. The hydrogel poly(-ethylene glycol) diacrylate was used to prepare structures for the replacement of cartilage [113]. Free-standing poly(ethylene glycol) diacrylate hydrogel scaffold fabricated by multiphoton lithography may also be used for neural tissue engineering. The proliferation of neuro2A cells on free-standing poly(ethylene glycol) diacrylate scaffolds was demonstrated; actin microfilaments, expression of β-tubulin neuronal marker, and multiple neuritic extensions per cell were noted [84].

In another study, μ-CT scans were used for multiphoton lithography of a trabecular-like framework similar to trabecular bone; this structure was called “Osteoprint.” SaOS-2 grown on the OrmoComp™ structures showed an upregulation of SaOS-2 cell maturation and increased osteogenic differentiation [115]. Multiphoton lithography was also used to create scaffolds from the zirconium Ormosil SZ2080; microstructured scaffolds containing hexagonal pores were shown to exhibit biocompatibility in a rabbit model similar to the commercially available collagen membranes [116].

Silicon-zirconium scaffolds with hexagonal chambers that are 50 μm in height and 100 μm in width were prepared out of the hybrid organic-inorganic (HOI) polymer SZ2080. The scaffolds were used to repair a murine osteochondral (bone) defect with a critical size of 3 mm in diameter and 2 mm in depth. The biocompatibility of the material was demonstrated using chondrocytes for up to 8 days; protein secretion and type II collagen gene upregulation was demonstrated. The scaffolds supported cartilage formation at 6 months [117]. A large-scale porous structure with a size of several millimeters was printed using multiphoton lithography (515 nm femtosecond laser) over 6.3 min from OrmoComp™; this result reflects a high printing rate for multiphoton lithography. A pore system from 10 μm to 90 μm was demonstrated; cell attachment was greater for scaffolds with larger pores [118]. Composite structures containing components that are not transparent to infrared light can be processed using 3D printing [119]; in the case of multiphoton lithography system, the small voxel size and the requirement for transparency limits the size of opaque particles in the photosensitive resin. A composite Ormocorp™ filled with opaque barium titanate nanoparticles has been prepared; a 3D scaffold with features that mimic the trabeculae of spongy bone was prepared using multiphoton lithography. The scaffolds exhibited enhanced differentiation of human SaOS-2 cells due to the piezoelectric effect associated with the nanoparticles [120]. The development of hybrid organic-inorganic transparent photoresins with a fully biodegradable and biocompatible network of P–O–P polyphosphate groups containing Ca^{2+} and Mg^{2+} cations [121] instead of a Si–O–Si framework could lead to a breakthrough in a bone tissue engineering by multiphoton lithography.

4.2. 3D printing rate

The 3D printing rate is dependent on the desired resolution and available processing time for processing macroscale scaffolds. A combination of one photon absorption and multiphoton absorption has been demonstrated, which enables a high scaffold fabrication speed [103]. Structures printed by two-photon absorption were surrounded by a rapidly fabricated ultraviolet laser ring. The ring can be fabricated by 1PA in seven minutes; in comparison, the ring can be fabricated by 2PA in 60 h. The permeability of the porous channels was demonstrated using rhodamine B solution [122].

Another approach for high speed fabrication of scaffolds for tissue engineering involves the use of a multi-focus multiphoton lithography technique [123]. Microporous biomimetic 3D niches, known as nichoids, for stem cell proliferation, were made using multi-focus approach with a spatial light modulator. Unlike a single-focus system, the multi-focus (6-foci) approach enables the production of a thicker structure at a higher rate and on a larger scale [123].

3D printing of porous scaffolds in a system with a long travel axis and a focusing system with a large working distance (NA = 0.45–0.60) was demonstrated. This approach enabled rapid writing speeds and a maximum structure height of several millimeters to be obtained [124]. Using Q-switched microchip in multiphoton lithography increases the printing rate up to 20 mm/s [125]. Adding a commercial resonant imaging mirror operating at 8 kHz enabled a 3D printing rate of up to ~ 8000 mm/s [126].

Centimeter-scale objects have been printed using a simultaneous spatiotemporal focusing (SSTF) approach [127]. This technique allows multiphoton lithography of 0.6–1.3 cm figures with a spatial resolution of 10–40 μm; in comparison, standard multiphoton lithography produces 0.1 cm scale structures with higher resolution (0.1 μm) [127]. The resolution of the printed structures can be increased by post processing, isotropic oxygen plasma etching, or pyrolysis at 690 °C [128].

The printing rate can be increased ten times using a Bessel beam with a line-shaped focus and a spatial light modulator. Unlike the ellipsoidal voxel of a Gaussian beam, this approach provides a conical wave front [129]. The use of a non-diffracting Bessel beam from a semiconductor light source has been described [130].

Multiphoton lithography requires an appropriate focus shape (spatially) and an appropriate level of peak power (temporally). The intensity of the beam can be increased spatially and temporally in the focal area by the objective. The objective can increase peak power by focusing the light; this process does not affect the pulse energy. In multiphoton lithography, temporal angular dispersion (or shortening of pulse duration) is performed via a collimator and objective lens [131]. Saha et al. recently described a projection-based parallel printing approach, which enabled the printing throughput to be increased by up to three orders of magnitude [131].

4.3. Resolution of a focal area

The multiphoton lithography printing rate can be confined by the voxel (focal area) and the resolution. Simultaneous spatiotemporal focusing of a femtosecond laser enables a structure with a maximum height of 0.6 cm to be prepared [127].

The small-diameter laser focus propagates by approximately 100 times the Rayleigh length with a chromatic focusing system and chirped laser pulses; the flying focus approach allows for decoupling of the speed at which the focus moves and the peak intensity from the group velocity of the laser [132]. Spherical aberrations decrease the peak intensity of the voxel, shift and expand the focal region on the way of the beam propagation, as well as decrease the quality and resolution of the printed structure; this phenomenon is associated with refraction at the air/glass interface. Possible shrinkage of the printed structure may be overcome by scaling the CAD model [133]. Millimeter sized scaffolds containing interconnected pores, several micrometer-sized voxels, and homogeneous features were created using medium numerical aperture air objectives that exhibit long working distances.

Laser energy with high intensity can lead to bubble formation in the polymer (damage threshold, P_{dam}) and an increase in voxel size; laser energy with lower intensity below the fabrication threshold cannot cause polymerization. The laser technique should be optimized for each photoresin [41]. For example, a tightly focused Ti: sapphire laser creates pulses with a wavelength of 780 nm and a repetition rate of 80 MHz (80 fs); these pulses are appropriate for processing inorganic-organic hybrid materials [134]. The resolution can be enhanced by using stimulated emission depletion (STED) technique [48,135,136]. Structures with lateral features of 55 nm have been printed using a tri- and tetra-acrylate mixture and a 7-diethylamino-3-thenoylcoumarin photoinitiator with this approach [135].

Structures with nanoscale features are needed to mimic the mosaic cone photoreceptor-like structures. A 63/1.4 NA objective was immersed into a drop of IP-S photoresist on the unpolished surface of a silicon wafer. Multiphoton lithography enabled processing of 5–10 μm tall photoreceptors [137]. By varying the laser focus position with respect to the glass substrate, features with a size below 100 nm may be obtained; a structure with a gap size of 65 nm and a periodic distance of 200 nm was demonstrated [138].

4.4. Chemistry of photoresins

Radical quenchers of polymerization reaction in photopolymers can be used to improve spatial resolution; however, the use of these materials is associated with a dramatic reduction in the elastic modulus of the scaffold [139]. Decreasing the femtosecond laser interaction time can also reduce the voxel size [140]. The resolution obtained from direct laser writing (DLW) system using two-photon polymerization is a ~7 nm width line; increasing the laser power ~80% can lead to the formation of 20 nm lines [141]. Photoinitiators should ideally exhibit short exposure times and high sensitivities [142]. The appropriate laser intensity for multiphoton absorption is determined by the chemistry of the photoresist. Highly reactive resins provide scans speeds up to 1000 mm/s; for structures with small-scale features, scan speeds of 0.1–1 mm/s are possible [41].

Photosensitive materials can be divided into (a) positive resists that are also used for photonics, lithography (e.g., AZP), templates, and liftoff (e.g., S1800) applications, (b) solid epoxy-based negative resists that are also used for photonics, lithography (e.g., SU-8), and templates (e.g., CAR44), and (c) liquid acrylate-based negative resists that are also used for biological applications, medical applications (e.g., PEGdma and SR499), MEMS, and other technological applications (e.g., Ormocer® materials) [143]. Most scaffolds created using multiphoton lithography are made out of negative photoresist precursors. Positive photoresist can be used for creating lines or other small-scale features [101,143–145]. The most commonly used positive photoresists are DNQ-novolac based compounds and polyimide positive photoresists [146–148]. Positive photoresists can be used for selectively removing regions within printed solid devices with high precision; however, these materials have limited usage in biomedical engineering to this point [149].

4.5. Cytotoxicity

Microfabrication of hydrogels requires efficient water-soluble photoinitiators (PI) [150–152]. Photoinitiators generally have the greatest influence on cytotoxicity [150]. Fig. 3 shows the relative viability of L929 fibroblasts that were exposed to the distilled water extract from polyethylene glycol diacrylate (SR610, Sartomer, Paris, France) samples, which were prepared with 0.5% and 2% of the photoinitiator Irgacure 2959. Fig. 3 indicates that higher concentrations of the photoinitiator in the freshly made (i.e., aged in distilled water for 24 h) extract samples were associated with higher levels of cytotoxicity. Both the 2 wt% Irgacure 2959 and the 0.5 wt% Irgacure 2959 samples were shown to be cytotoxic. Aging the samples in distilled water for six additional days reduced the water-soluble toxic components to levels that were associated with no cytotoxic effect. This study indicated that the photoinitiator and other toxic components can be washed out of 2PP-fabricated structures, providing a fully biocompatible PEGda material. In another study, hydrogel structures were prepared with the new photoinitiators cyclohexanone initiators (E2CK) and cyclopentanone initiators (P2CK), which were synthesized via aldol condensation. The initiators were dissolved in phosphate-buffered saline; biocompatibility using osteosarcoma cells MG-63 and outgrowth endothelial cells (OEC) was demonstrated. The average speed for processing hydrogels with a grid structure was 100 mm/s [153].

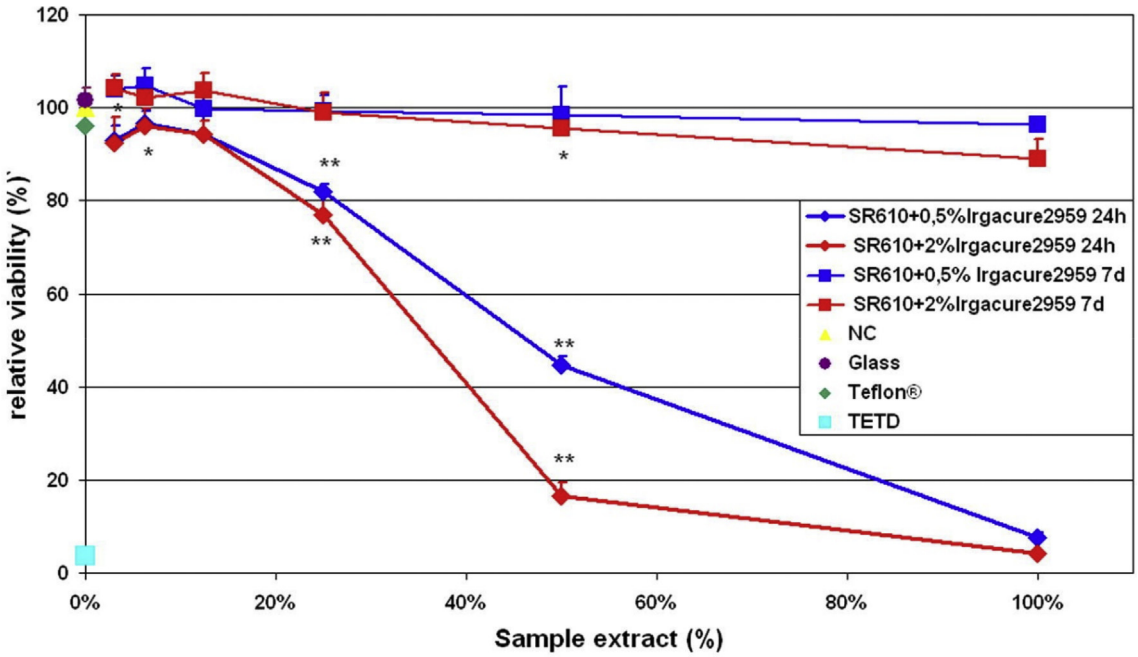

Fig. 3. (a) Relative viability of L929 fibroblasts in response to extract obtained from freshly prepared (24 h) and aged (7 day) SR610 samples, which contain Irgacure 2959 photoinitiator in 0.5% and 2% concentrations. (b) Relative viability of L929 fibroblasts in direct contact with freshly prepared (24 h) and aged (7 day) samples. For both tests, relative cell viability correlates inversely with the amount of photoinitiator. Reproduced with permission from Ref. [150].

Common benzylidene ketone dyes are highly efficient water-soluble photoinitiators; however, they exhibit cytotoxic properties [154–156]. To prevent migration of the photoinitiator, the photoinitiator was bound to the polymeric hyaluronan backbone of the printed hydrogel (HAPI, ω (H_2O) = 85%). An absence of cytotoxicity was demonstrated using MC3T3 cells [154]. Modified water-soluble benzylidene cyclanone dyes showed biocompatibility in a MTT assay with HepG2 cells [155]. In another study, water-dispersible nanoparticles of the water-insoluble photoinitiator, 2,4,6-trimethylbenzoyl-diphenylphosphine oxide (TPO), were prepared via rapid conversion of a microemulsion into a water-dispersible powder. The extinction coefficient of these materials was 300 times greater than those of commercially-available water--soluble photoinitiators; rapid polymerization rates were demonstrated using this approach. Huh7 liver cells were cultured on different 3D substrates made from this material [156].

The backbone of a printed hydrogel must exhibit an appropriate level of biocompatibility. The chitosan backbone (CHGM) showed appropriate biocompatibility with HPMEC cells. A printed 3D ring microstructure made from this material showed appropriate stiffness (1–10 kPa) for cell studies; the stiffness value is dependent on the PEGDA cross-linker concentration [157]. Another backbone is tyramine-substituted hyaluronan (HA-Tyr) hydrogel; a high rate of human mesenchymal stromal cell (hMSC) viability was demonstrated on microstructures made of this material [158].

The biocompatibility of a polymer containing poly(ethylene glycol) and poly(acrylic acid) (PEG/PAA) interpenetrating network was studied in rabbit cornea. The cornea remained clear at 16 months; however, a large number of complications were observed [159]. In another study, multiphoton lithography was performed using a tetrafunctional acrylic monomer and a tetrafunctional thiol; processing of this material was associated with a higher fabrication speed [160]. Moreover, this material showed lower levels of shrinkage and higher levels of crosslinking than conventional materials. High viscosity acrylic resins were shown to require more power for printing at the same resolution [161].

Gelatin methacryloyl (GelMA) hydrogels were processed with the commercial Irgacure® 2959 photoinitiator using near-UV irradiation. This material shows biocompatibility at low concentrations [162]. In another study, gelatin methacrylamide hydrogel was processed using multiphoton lithography; this material was shown to support adhesion, differentiation, and proliferation of adipose-derived stem cells [163]. Moreover, the polymerized material was shown to undergo enzymatic degradation.

In more recent studies, alternative chemistries for photopolymerization-based processing have been described. For example, allylated gelatin (GelAGE) was shown to be compatible with thiol–ene clickable processing; this material was shown to be compatible with digital light processing-based 3D printing and encapsulation of chondrocytes. Unlike GelMA, GelAGE fully biodegradable GelMA [164]. In another study, the visible light photoinitiator ruthenium (Ru)/sodium persulfate (SPS) was used to process gelatin-methacryloyl (Gel-MA)-based hydrogel. This material showed better cell viability rates than the material that processed using the conventional photoinitiator Irgacure 2959 [165].

Visible light polymerization can be obtained using eosin-Y photoinitiator for gelation of thiol-norbornene hydrogels. The biocompatibility of this material was demonstrated using hMSCs and MIN6 β –cells [166]. In another study, the gelatin methacryloyl backbone was modified with sodium alginate; cross-linking of the hydrogel network can occur through ionic, physical, and covalent methods as well as through reactions with Ca^{2+} ions. High levels of cell proliferation were demonstrated on materials with high levels of gelatin and low levels of alginate [167].

The cell encapsulation process, which involves incorporating the cells within the scaffolds during the multiphoton lithography process, can be used as an alternative to seeding cells on already-prepared scaffolds. This approach enables higher cell densities and more a uniform distribution of cells within the scaffold. One of the issues associated with the cell encapsulation process is the cytotoxicity of many photoinitiators (2PI). The water-soluble cleavable diazo sulfonate was developed to overcome this limitation. Samples were prepared using 10% gelatin methacrylamide hydrogel with 1 mM P2CK or 2 mM diazo sulfonate (Fig. 4 (I)). A cell cytotoxicity assay showed better cell viability for samples prepared with diazo sulfonate (Fig. 4 (II)). At high concentrations, diazo sulfonate was able to support a printing rate of up to 1 m/s [168]. L929 fibroblasts and MC3T3 preosteoblasts showed good cell viability rates

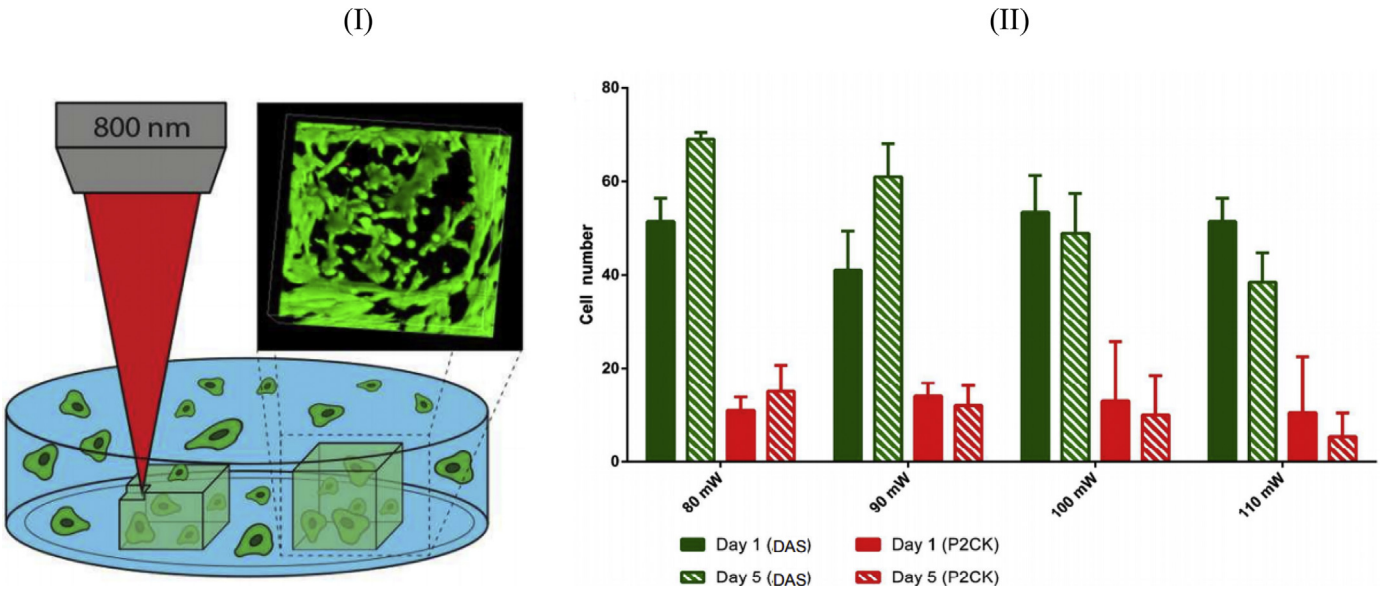

Fig. 4. (I) Scheme of multiphoton lithography process. The survival and proliferation of ASC/TERT1 cells in multiphoton lithography-produced gelatin methacrylamide hydrogel constructs are also shown. The dimensions of the cells encapsulated model are 500 μm × 500 μm x 125 μm. (II) The number of cells within the 3D printed hydrogel cubes at day 1 and day 5. The use of DAS as a photoinitiator resulted in a higher initial higher cell survival and increased proliferation rate than P2CK. Reproduced with permission from Ref. [167].

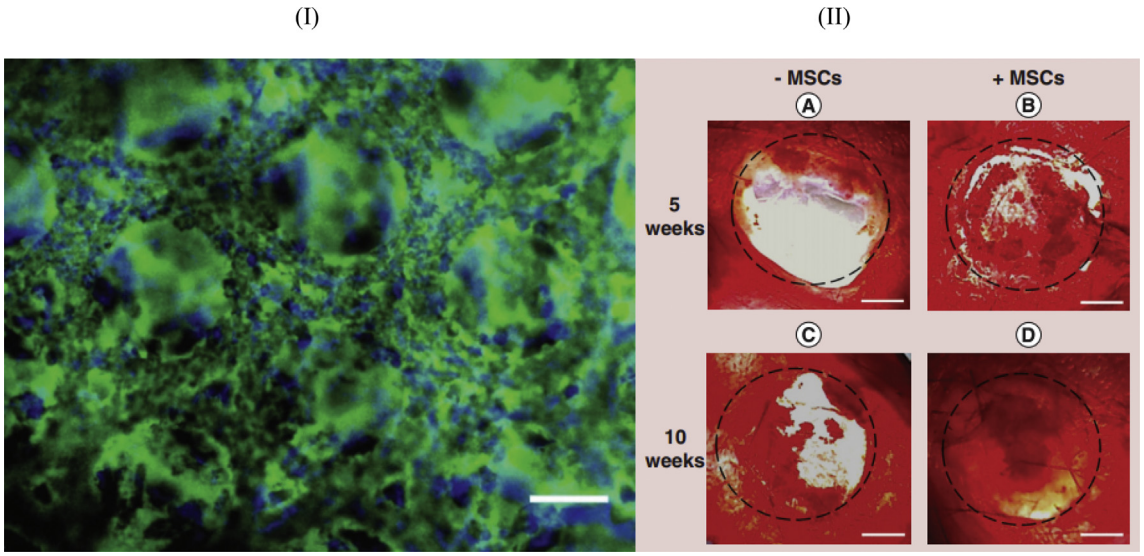

Fig. 5. (I) Analysis of the star-shaped poly(D,L-lactide) scaffold cytotoxicity *via* qualitative live/dead staining 24 h post-seeding using optical phase-contrast microscopy. A combination of Hoechst (cell nuclei) and calcein (live cells)/propidium iodide (dead cells) staining was used; the lack of red zones indicates that the cells are living. The scale bar is 75 μm. (II) Alizarin Red S analysis of the harvested bones with the star-shaped poly(D,L-lactide) scaffolds after 5 and 10 weeks. The dashed line indicates the area of the formed defect. Alizarin Red S staining was localized mineralized tissue; the red-colored area inside the formed defect indicates the zone of mineralization. (A) MSC(−) scaffolds after 5 weeks, (B) MSC(+) scaffolds after 5 weeks, (C) MSC(−) scaffolds after 10 weeks, (D) MSC(+) scaffolds after 10 weeks. The scale bars are 1 mm for all of the images. MSC: Mesenchymal stem cell. Reproduced with permission from Ref. [174]. (For interpretation of the references to color in this figure legend, the reader is referred to the Web version of this article.)

when exposed to the hydrogel gelatin-methacrylamide (gel-MOD) that was modified with 2-aminoethyl methacrylate (AEMA) [169]. The material showed less swelling (0–20%) than gel-MOD (75–100%).

Gelatin-based hydrogel scaffolds were prepared using multiphoton lithography via the highly reactive norbornene (Gel-NB) modification. This modification enables subsequent thiol-ene photo-click crosslinking for multiphoton lithography fabrication of scaffolds [170]. In another study, a number of scaffolds were prepared out of a nontoxic insoluble Zr–Si compound; macroporous (150–250 μm) scaffolds that were prepared from this material were studied using human bone marrow stem cells and human adipose tissue-derived stem cells. Human adipose tissue derived stem cells and human bone marrow stem cells that were cultured in osteoinductive and control media for twenty-one days were shown to deposit calcium phosphate (Fig. 6); however, these scaffolds may not be entirely appropriate for tissue engineering since they are not bioresorbable [171].

4.6. Bioresorbability of scaffolds and microdevices

Scaffolds for bone tissue engineering should be biocompatible and

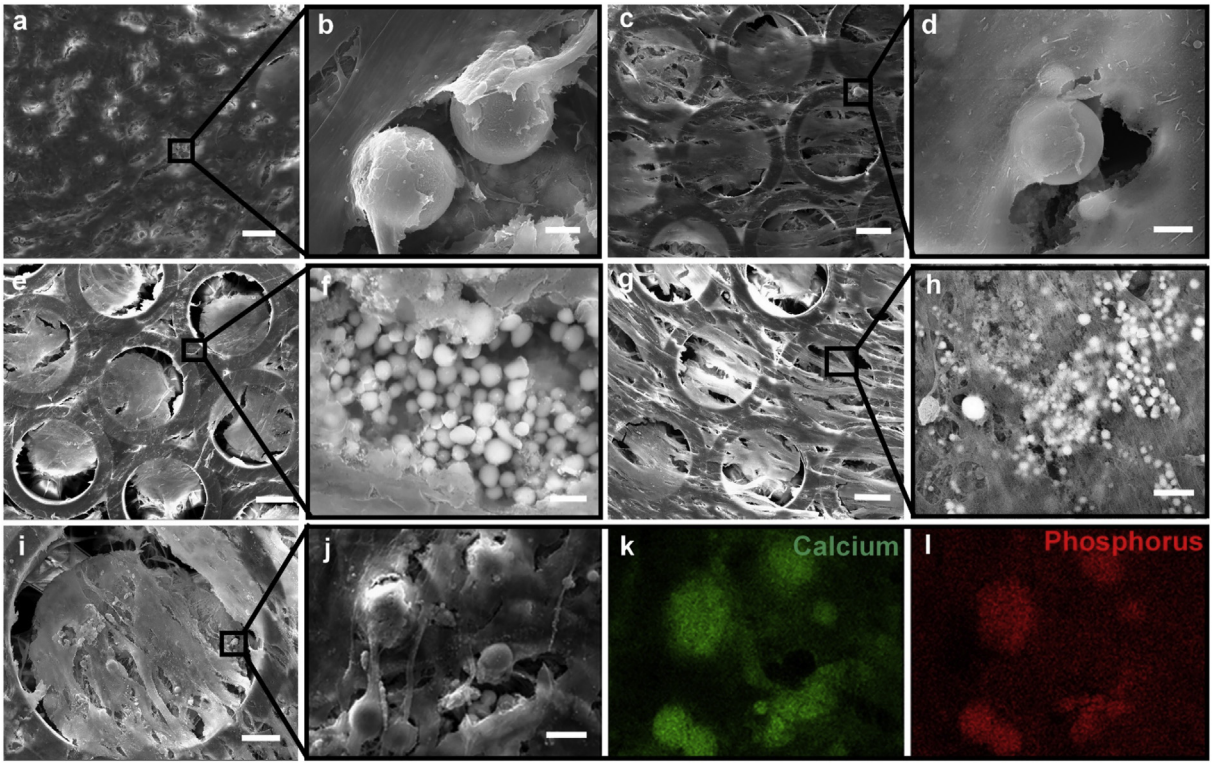

Fig. 6. High magnification images showing calcium phosphate deposits of hASCs and hBMSCs cultured on Zr–Si scaffolds in osteogenic (b and d) and control (f and h) conditions; (i–l) EDX mapping confirming the presence of calcium and phosphor in the accumulations. Scale bars: (a, c, e, g) 60 μm, (b, d, f, h) 5 μm, (i) 50 μm and (j–l) 10 μm. Reproduced from Koroleva A, Deiwick A, Nguyen A, Schlie-Wolter S, Narayan R, Timashev P, Popov V, Bagratashvili V, Chichkov B. Osteogenic differentiation of human mesenchymal stem cells in 3-D Zr–Si organic-inorganic scaffolds produced by two-photon polymerization technique. PloS one. 2015; 10(2). This work is subject to Creative Commons Attribution (CC BY) license.

resorbable. The main requirements for scaffolds include the following: (I) an interconnected vascular network; (II) biocompatibility, an absence of immune response, and an appropriate biodegradation rate; (III) suitable properties to support the proliferation of cells and integration with the surrounding soft tissue; and (IV) mechanical properties similar to those of the native tissue at the implantation site. The degradation of a tissue engineering scaffold is associated with (I) degradation, (II) bulk erosion, as well as (III) resorption processes. All of these steps are accompanied by novel tissue formation. The materials, structure, and presence of cells in the scaffold determinate the remodeling rate [172].

Another problem is to produce biodegradable photoresins for multiphoton lithography [173]. Scaffolds made of methacrylated polylactide, methacrylated polycaprolactone, or hyaluronic acid glycidyl methacrylate are preferable due to their biodegradation properties [174]. A macroporous (300 μm) scaffold with a Schwarz primitive minimal surface was prepared out of poly(D,L-lactide-co-ϵ-caprolactone) copolymer via ring-opening-polymerization and photoactivation using multiphoton lithography. The processing rate was limited to equal 1 cm^3 of scaffold per day of printing. The half-life of the scaffolds was over a range from 100 to 300 days at 37 °C; it was dependent on the amount of polylactide in the scaffold [27]. 3D scaffolds were also fabricated from a star-shaped poly(D, L-lactide) using multiphoton lithography; human adipose-derived stem cells were subsequently grown on the scaffold (Fig. 5). The mesenchymal stem cells showed good adhesion properties to the scaffold, an absence of cytotoxicity in the scaffold environment, and biomineralization. The Young's modulus of the scaffold was greater than 6 GPa [175]. In addition, scaffolds for tissue engineering were fabricated using the combination of laser-induced forward transfer (LIFT) and multiphoton lithography. LIFT was used for directing cell seeding; this approach provided control over cell density and position [176].

5. Conclusions

Multiphoton lithography has unique capabilities for the fabrication of tissue engineering scaffolds as well as microdevices such as biomedical microneedles, microfilters, and probes. Although multiphoton lithography is uniquely capable of 3D printing tissue engineering scaffolds with sub-micrometer scale features, this approach is associated with long processing rates. Other limitations associated with this approach include the requirement for near-infrared transparent resins to avoid scattering and attenuation of photons by the photoresist. The poor biocompatibility of many of the materials used in multiphoton lithography is another limitation. Recent studies have described innovative photoresists for multiphoton lithography, novel chromophores for high resolution lithography, more efficient photoinitiators, and multiphoton lithography of bioresorbable scaffolds. The bioresorbable materials used in multiphoton lithography will need to be optimized in terms of stiffness, biodegradation rate, and porosity for each tissue type prior to translation for clinical use [177]. Despite the current limitations of multiphoton lithography technology, recent studies indicate pathways for the translation of tissue engineering scaffolds with clinically-relevant dimensions at commercially viable processing rates.

Declaration of competing interest

The authors declare that they have no known competing financial interests or personal relationships that could have appeared to influence the work reported in this paper.

Acknowledgements

Mr. Zuev wishes to acknowledge support from the Fulbright program at the Institute of International Education. Dr. Narayan wishes to

acknowledge support from National Science Foundation Award #1762202.

References

[1] M. Göppert-Mayer, Elementary processes with two quantum transitions, Ann. Phys. 18 (7-8) (2009 Aug 11) 466–479.
[2] E.T. Ritschdorff, R. Nielson, J.B. Shear, Multi-focal multiphoton lithography, Lab Chip 12 (5) (2012) 867–871.
[3] W. Haske, V.W. Chen, J.M. Hales, W. Dong, S. Barlow, S.R. Marder, J.W. Perry, 65 nm feature sizes using visible wavelength 3-D multiphoton lithography, Optic Express 15 (6) (2007 Mar 19) 3426–3436.
[4] S. Hunter, F. Kiamilev, S. Esener, D.A. Parthenopoulos, P.M. Rentzepis, Potentials of two-photon based 3-D optical memories for high performance computing, Appl. Optic. 29 (14) (1990 May 10) 2058–2066.
[5] D.A. Parthenopoulos, P.M. Rentzepis, Three-dimensional optical storage memory, Science 245 (4920) (1989 Aug 25) 843–845.
[6] J. Qiu, K. Miura, K. Hirao, Three-dimensional optical memory using glasses as a recording medium through a multi-photon absorption process, Jpn. J. Appl. Phys. 37 (4S) (1998 Apr) 2263.
[7] H.B. Sun, S. Kawata, Two-photon photopolymerization and 3D lithographic microfabrication, in: NMR• 3D Analysis• Photopolymerization, Springer, Berlin, Heidelberg, 2004, pp. 169–273.
[8] M.A. Unger, H.P. Chou, T. Thorsen, A. Scherer, S.R. Quake, Monolithic microfabricated valves and pumps by multilayer soft lithography, Science 288 (5463) (2000 Apr 7) 113–116.
[9] D.J. Ehrlich, J.Y. Tsao (Eds.), Laser Microfabrication: Thin Film Processes and Lithography, Elsevier, 1989 Jun 21.
[10] W. Jung, S. Tang, D.T. McCormic, T. Xie, Y.C. Ahn, J. Su, I.V. Tomov, T.B. Krasieva, B.J. Tromberg, Z. Chen, Miniaturized probe based on a microelectromechanical system mirror for multiphoton microscopy, Optic. Lett. 33 (12) (2008 Jun 15) 1324–1326.
[11] D. Kim, P.T. So, High-throughput three-dimensional lithographic microfabrication, Optic. Lett. 35 (10) (2010 May 15) 1602–1604.
[12] Y. Lu, F. Hasegawa, T. Goto, S. Ohkuma, S. Fukuhara, Y. Kawazu, K. Totani, T. Yamashita, T. Watanabe, Highly sensitive two-photon chromophores applied to three-dimensional lithographic microfabrication: design, synthesis and characterization towards two-photon absorption cross section, J. Mater. Chem. 14 (1) (2004) 75–80.
[13] S. Maruo, J.T. Fourkas, Recent progress in multiphoton microfabrication, Laser Photon. Rev. 2 (1-2) (2008 Apr 25) 100–111.
[14] R. Nielson, B. Kaehr, J.B. Shear, Microreplication and design of biological architectures using dynamic-mask multiphoton lithography, Small 5 (1) (2009 Jan) 120–125.
[15] A.M. Kasko, D.Y. Wong, Two-photon lithography in the future of cell-based therapeutics and regenerative medicine: a review of techniques for hydrogel patterning and controlled release, Future Med. Chem. 2 (11) (2010 Nov) 1669–1680.
[16] J.F. Xing, M.L. Zheng, X.M. Duan, Two-photon polymerization microfabrication of hydrogels: an advanced 3D printing technology for tissue engineering and drug delivery, Chem. Soc. Rev. 44 (15) (2015) 5031–5039.
[17] P. Bajaj, R.M. Schweller, A. Khademhosseini, J.L. West, R. Bashir, 3D biofabrication strategies for tissue engineering and regenerative medicine, Annu. Rev. Biomed. Eng. 16 (2014 Jul 11) 247–276.
[18] J. Stampfl, R. Liska, A. Ovsianikov, Multiphoton Lithography: Techniques, Materials, and Applications, John Wiley & Sons, 2016 Dec 19.
[19] M. Malinauskas, V. Purlys, M. Rutkauskas, A. Gaidukevičiūtė, R. Gadonas, Femtosecond visible light induced two-photon photopolymerization for 3D micro/nanostructuring in photoresists and photopolymers, Lith. J. Phys. 50 (2) (2010 Apr 1).
[20] Q. Guo, R. Ghadiri, T. Weigel, A. Aumann, E.L. Gurevich, C. Esen, O. Medenbach, W. Cheng, B. Chichkov, A. Ostendorf, Comparison of in situ and ex situ methods for synthesis of two-photon polymerization polymer nanocomposites, Polymers 6 (7) (2014 Jul) 2037–2050.
[21] U. Staudinger, G. Zyla, B. Krause, A. Janke, D. Fischer, C. Esen, B. Voit, A. Ostendorf, Development of electrically conductive microstructures based on polymer/CNT nanocomposites via two-photon polymerization, Microelectron. Eng. 179 (2017 Jul 5) 48–55.
[22] J. Serbin, A. Ovsianikov, B. Chichkov, Fabrication of woodpile structures by two-photon polymerization and investigation of their optical properties, Optic Express 12 (21) (2004 Oct 18) 5221–5228.
[23] K.S. Lee, D.Y. Yang, S.H. Park, R.H. Kim, Recent developments in the use of two-photon polymerization in precise 2D and 3D microfabrications, Polym. Adv. Technol. 17 (2) (2006 Feb) 72–82.
[24] C. Koos, P. Vorreau, T. Vallaitis, P. Dumon, W. Bogaerts, R. Baets, B. Esembeson, I. Biaggio, T. Michinobu, F. Diederich, W. Freude, All-optical high-speed signal processing with silicon–organic hybrid slot waveguides, Nat. Photon. 3 (4) (2009 Apr) 216.
[25] M. Bouillard, G. Boucher, J.F. Ortas, B. Kanseri, R. Tualle-Brouri, High production rate of single-photon and two-photon Fock states for quantum state engineering, Optic Express 27 (3) (2019 Feb 4) 3113–3120.
[26] D. Perevoznik, K. Kurselis, R. Kiyan, E.K. Nepomnyashchaya, E.T. Aksenov, E.N. Velichko, B.N. Chichkov, 3D printing of polymer structures by two-photon polymerization using Q-switched microchip laser, in: Progress in Electromagnetics Research Symposium-Spring (PIERS) 2017 May 22, IEEE, 2017, pp. 2313–2315.
[27] R.M. Felfel, L. Poocza, M. Gimeno-Fabra, T. Milde, G. Hildebrand, I. Ahmed, C. Scotchford, V. Sottile, D.M. Grant, K. Liefeith, In vitro degradation and mechanical properties of PLA-PCL copolymer unit cell scaffolds generated by two-photon polymerization, Biomed. Mater. 11 (1) (2016 Feb 2), 015011.
[28] A.K. Nguyen, S.D. Gittard, A. Koroleva, S. Schlie, A. Gaidukeviciute, B.N. Chichkov, R.J. Narayan, Two-photon polymerization of polyethylene glycol diacrylate scaffolds with riboflavin and triethanolamine used as a water-soluble photoinitiator, Regen. Med. 8 (6) (2013 Nov) 725–738.
[29] Boyd RW. Nonlinear Optics, 436–440.
[30] J.D. Bhawalkar, G.S. He, P.N. Prasad, Nonlinear multiphoton processes in organic and polymeric materials, Rep. Prog. Phys. 59 (9) (1996 Sep) 1041.
[31] J. Lin, X. Jing, X. Zhou, X. Zheng, R. Gao, Y. Wang, Scaling laws of nanorods in two-photon polymerization nanofabrication using a continuous scanning method, AIP Adv. 6 (10) (2016 Oct 27) 105014.
[32] M. Bass, Handbook of Optics: Fundamentals, Techniques, and Design, McGraw-Hill Professional, 1994 Sep 1.
[33] D. Schimpf, Pulse-shaping strategies in short-pulse fiber amplifiers, Doctoral dissertation, PhD thesis, Friedrich-Schiller University, 2010.
[34] B. Kaehr, J.B. Shear, High-throughput design of microfluidics based on directed bacterial motility, Lab Chip 9 (18) (2009) 2632–2637.
[35] S. Maruo, K. Ikuta, H. Korogi, Force-controllable, optically driven micromachines fabricated by single-step two-photon microstereolithography, J. Microelectromech. Syst. 12 (5) (2003 Oct 27) 533–539.
[36] S. Maruo, H. Inoue, Optically driven micropump produced by three-dimensional two-photon microfabrication, Appl. Phys. Lett. 89 (14) (2006 Oct 2) 144101.
[37] P. Galajda, P. Ormos, Complex micromachines produced and driven by light, Appl. Phys. Lett. 78 (2) (2001 Jan 8) 249–251.
[38] Q. Geng, D. Wang, P. Chen, S.C. Chen, Ultrafast multi-focus 3-D nano-fabrication based on two-photon polymerization, Nat. Commun. 10 (1) (2019 May 16) 1–7.
[39] L. Li, J.T. Fourkas, Multiphoton polymerization, Mater. Today 10 (6) (2007 Jun 1) 30–37.
[40] J.D. Bhawalkar, N.D. Kumar, C.F. Zhao, P. Prasad, Two-photon photodynamic therapy, J. Clin. Laser Med. Surg. 15 (5) (1997) 201–204.
[41] S.C. Ligon, R. Liska, J. Stampfl, M. Gurr, R. Mülhaupt, Polymers for 3D printing and customized additive manufacturing, Chem. Rev. 117 (15) (2017 Aug 9) 10212–10290.
[42] R. Houbertz, P. Declerck, S. Passinger, A. Ovsianikov, J. Serbin, B.N. Chichkov, Investigations on the generation of photonic crystals using two-photon polymerization (2PP) of inorganic–organic hybrid polymers with ultra-short laser pulses, Phys. Status Solidi 204 (11) (2007 Nov) 3662–3675.
[43] B.H. Cumpston, S.P. Ananthavel, S. Barlow, D.L. Dyer, J.E. Ehrlich, L.L. Erskine, A.A. Heikal, S.M. Kuebler, I.Y. Lee, D. McCord-Maughon, J. Qin, Two-photon polymerization initiators for three-dimensional optical data storage and microfabrication, Nature 398 (6722) (1999 Mar) 51–54.
[44] Y.C. Chen, J.L. Ferracane, S.A. Prahl, Quantum yield of conversion of the photoinitiator camphorquinone, Dent. Mater. 23 (6) (2007 Jun 1) 655–664.
[45] K.J. Schafer, J.M. Hales, M. Balu, K.D. Belfield, E.W. Van Stryland, D.J. Hagan, Two-photon absorption cross-sections of common photoinitiators, J. Photochem. Photobiol. Chem. 162 (2–3) (2004 Mar 15) 497–502.
[46] L.M. Maestro, E.M. Rodriguez, F. Vetrone, R. Naccache, H.L. Ramirez, D. Jaque, J.A. Capobianco, J.G. Solé, Nanoparticles for highly efficient multiphoton fluorescence bioimaging, Optic Express 18 (23) (2010 Nov 8) 23544–23553.
[47] M. Pawlicki, H.A. Collins, R.G. Denning, H.L. Anderson, Two-photon absorption and the design of two-photon dyes, Angew. Chem. Int. Ed. 48 (18) (2009 Apr 20) 3244–3266.
[48] X. Zhou, Y. Hou, J. Lin, A review on the processing accuracy of two-photon polymerization, AIP Adv. 5 (3) (2015 Mar 31), 030701.
[49] B. Valeur, Molecular fluorescence, Digital Encyclopedia of Applied Physics (2003 Apr 15) 477–531.
[50] J. Serbin, A. Egbert, A. Ostendorf, B.N. Chichkov, R. Houbertz, G. Domann, J. Schulz, C. Cronauer, L. Fröhlich, M. Popall, Femtosecond laser-induced two-photon polymerization of inorganic–organic hybrid materials for applications in photonics, Optic. Lett. 28 (5) (2003 Mar 1) 301–303.
[51] K. Sugioka, Y. Cheng, Ultrafast lasers—reliable tools for advanced materials processing, Light Sci. Appl. 3 (4) (2014 Apr) e149.
[52] M. Emons, K. Obata, T. Binhammer, A. Ovsianikov, B.N. Chichkov, U. Morgner, Two-photon polymerization technique with sub-50 nm resolution by sub-10 fs laser pulses, Opt. Mater. Express 2 (7) (2012 Jul 1) 942–947.
[53] A. Pe'er, B. Dayan, M. Vucelja, Y. Silberberg, A.A. Friesem, Quantum lithography by coherent control of classical light pulses, Optic Express 12 (26) (2004 Dec 27) 6600–6605.
[54] P. Pozzi, D. Gandolfi, M. Tognolina, G. Chirico, J. Mapelli, E. D'Angelo, High-throughput spatial light modulation two-photon microscopy for fast functional imaging, Neurophotonics 2 (1) (2015 Feb), 015005.
[55] F. Jipa, M. Zamfirescu, A. Velea, M. Popescu, R. Dabu, Femtosecond laser lithography in organic and non-organic materials, Updates in Advanced Lithography (2013 Jul 3) 3.
[56] C. Ibáñez-López, G. Saavedra, G. Boyer, M. Martínez-Corral, Quasi-isotropic 3-D resolution in two-photon scanning microscopy, Optic Express 13 (16) (2005 Aug 8) 6168–6174.
[57] S.D. Gittard, A. Ovsianikov, B.N. Chichkov, A. Doraiswamy, R.J. Narayan, Two-photon polymerization of microneedles for transdermal drug delivery, Expet Opin. Drug Deliv. 7 (4) (2010 Apr 1) 513–533.
[58] S.N. Economidou, D.A. Lamprou, D. Douroumis, 3D printing applications for transdermal drug delivery, Int. J. Pharm. 544 (2) (2018 Jun 15) 415–424.

[59] M. Suzuki, T. Takahashi, S. Aoyagi, 3D laser lithographic fabrication of hollow microneedle mimicking mosquitos and its characterisation, Int. J. Nanotechnol. 15 (1–3) (2018) 157–173.

[60] C. Plamadeala, S.R. Gosain, S. Purkhart, B. Buchegger, W. Baumgartner, J. Heitz, Three-Dimensional photonic structures fabricated by two-photon polymerization for microfluidics and microneedles, in: 20th International Conference on Transparent Optical Networks (ICTON) 2018 Jul 1, IEEE, 2018, pp. 1–4.

[61] H.S. Santana, M.S. Palma, M.G. Lopes, J. Souza, G.A. Lima, O.P. Taranto, J.L. Silva Jr., Microfluidic devices and 3D printing for synthesis and screening of drugs and tissue engineering, Ind. Eng. Chem. Res. 59 (9) (2019 Sep 18) 3794–3810.

[62] D. Mandt, P. Gruber, M. Markovic, M. Tromayer, M. Rothbauer, S.R. Kratz, S.F. Ali, J. Van Hoorick, W. Holnthoner, S. Muehleder, P. Dubruel, Fabrication of biomimetic placental barrier structures within a microfluidic device utilizing two-photon polymerization, Int. J. Bioprinting 4 (2) (2018).

[63] B. Xu, W. Hu, W. Du, Y. Hu, C. Zhang, Z. Lao, J. Ni, J. Li, D. Wu, J. Chu, K. Sugioka, Arch-like microsorters with multi-modal and clogging-improved filtering functions by using femtosecond laser multifocal parallel microfabrication, Optic Express 25 (14) (2017 Jul 10) 16739–16753.

[64] S.D. Gittard, A. Nguyen, K. Obata, A. Koroleva, R.J. Narayan, B.N. Chichkov, Fabrication of microscale medical devices by two-photon polymerization with multiple foci via a spatial light modulator, Biomed. Optic Express 2 (11) (2011 Nov 1) 3167–3178.

[65] A. Zakhurdaeva, P.I. Dietrich, H. Hölscher, C. Koos, J.G. Korvink, S. Sharma, Custom-designed glassy carbon tips for atomic force microscopy, Micromachines 8 (9) (2017 Sep) 285.

[66] G. Göring, P.I. Dietrich, M. Blaicher, S. Sharma, J.G. Korvink, T. Schimmel, C. Koos, H. Hölscher, Tailored probes for atomic force microscopy fabricated by two-photon polymerization, Appl. Phys. Lett. 109 (6) (2016 Aug 8), 063101.

[67] J. Bauer, A. Schroer, R. Schwaiger, O. Kraft, Approaching theoretical strength in glassy carbon nanolattices, Nat. Mater. 15 (4) (2016 Apr) 438–443.

[68] N. Schierbaum, J. Rheinlaender, T.E. Schäffer, Combined atomic force microscopy (AFM) and traction force microscopy (TFM) reveals a correlation between viscoelastic material properties and contractile prestress of living cells, Soft Matter 15 (8) (2019) 1721–1729.

[69] D.M. Zuev, E.S. Klimashina, P.V. Evdokimov, Y.Y. Filippov, V.I. Putlyaev, Preparation of β-Ca $_3$ (PO $_4$) $_2$/poly (D, L-lactide) and β-Ca $_3$ (PO $_4$) $_2$/poly (ε-caprolactone) biocomposite implants for bone substitution, Inorg. Mater. 54 (1) (2018 Jan 1) 87–95.

[70] D.M. Zuev, E.S. Klimashina, P.V. Evdokimov, Y.Y. Filippov, V.I. Putlyaev, Mechanical characteristics of composites based on β-Ca $_3$ (PO $_4$) 2/poly (D, L-lactide) and β-Ca $_3$ (PO $_4$) $_2$/poly (ε-Caprolactone), Inorg. Mater.: Appl. Res. 10 (1) (2019 Jan 1) 109–113.

[71] V.I. Putlyaev, P.V. Evdokimov, T.V. Safronova, E.S. Klimashina, N.K. Orlov, Fabrication of osteoconductive Ca $_{3-x}$ M 2x (PO $_4$) $_2$ (M= Na, K) calcium phosphate bioceramics by stereolithographic 3D printing, Inorg. Mater. 53 (5) (2017 May 1) 529–535.

[72] S. Azizi Machekposhti, S. Mohaved, R.J. Narayan, Inkjet dispensing technologies: recent advances for novel drug discovery, Expet Opin. Drug Discov. 14 (2) (2019 Feb 1) 101–113.

[73] X. Cui, K. Breitenkamp, M.G. Finn, M. Lotz, D.D. D'Lima, Direct human cartilage repair using three-dimensional bioprinting technology, Tissue Eng. 18 (11–12) (2012 Jun 1) 1304–1312.

[74] H.W. Kang, S.J. Lee, I.K. Ko, C. Kengla, J.J. Yoo, A. Atala, A 3D bioprinting system to produce human-scale tissue constructs with structural integrity, Nat. Biotechnol. 34 (3) (2016 Mar) 312.

[75] I.A. Paun, R.C. Popescu, C.C. Mustaciosu, M. Zamfirescu, B.S. Calin, M. Mihailescu, M. Dinescu, A. Popescu, D. Chioibasu, M. Soproniy, C.R. Luculescu, Laser-direct writing by two-photon polymerization of 3D honeycomb-like structures for bone regeneration, Biofabrication 10 (2) (2018 Feb 5), 025009.

[76] I.A. Paun, M. Zamfirescu, C.R. Luculescu, A.M. Acasandrei, C.C. Mustaciosu, M. Mihailescu, M. Dinescu, Electrically responsive microreservoires for controllable delivery of dexamethasone in bone tissue engineering, Appl. Surf. Sci. 392 (2017 Jan 15) 321–331.

[77] E.A. Neel, A. Aljabo, A. Strange, S. Ibrahim, M. Coathup, A.M. Young, L. Bozec, V. Mudera, Demineralization–remineralization dynamics in teeth and bone, Int. J. Nanomed. 11 (2016) 4743.

[78] M.M. Nava, T. Zandrini, G. Cerullo, R. Osellame, M.T. Raimondi, 3D Stem Cell Niche Engineering via Two-Photon Laser Polymerization. In3D Cell Culture, Humana Press, New York, NY, 2017, pp. 253–266.

[79] E.D. Lemma, B. Spagnolo, M. De Vittorio, F. Pisanello, Studying cell mechanobiology in 3D: the two-photon lithography approach, Trends Biotechnol. 37 (4) (2019 Apr 1) 358–372.

[80] P. Tayalia, C.R. Mendonca, T. Baldacchini, D.J. Mooney, E. Mazur, 3D cell-migration studies using two-photon engineered polymer scaffolds, Adv. Mater. 20 (23) (2008 Dec 2) 4494–4498.

[81] J.S. Oakdale, J. Ye, W.L. Smith, J. Biener, Post-print UV curing method for improving the mechanical properties of prototypes derived from two-photon lithography, Optic Express 24 (24) (2016 Nov 28) 27077–27086.

[82] S.H. Lee, J.J. Moon, J.L. West, Three-dimensional micropatterning of bioactive hydrogels via two-photon laser scanning photolithography for guided 3D cell migration, Biomaterials 29 (20) (2008 Jul 1) 2962–2968.

[83] K. Parkatzidis, M. Chatzinikolaidou, M. Kaliva, A. Bakopoulou, M. Farsari, M. Vamvakaki, Multiphoton 3D printing of biopolymer-based hydrogels, ACS Biomater. Sci. Eng. 5 (11) (2019 Oct 15) 6161–6170.

[84] A. Accardo, M.C. Blatché, R. Courson, I. Loubinoux, C. Vieu, L. Malaquin, Two-photon lithography and microscopy of 3D hydrogel scaffolds for neuronal cell growth, Biomed. Phys. Eng. Express 4 (2) (2018 Feb 16), 027009.

[85] L. Gao, M.E. Kupfer, J.P. Jung, L. Yang, P. Zhang, Y. Da Sie, Q. Tran, V. Ajeti, B.T. Freeman, V.G. Fast, P.J. Campagnola, Myocardial tissue engineering with cells derived from human-induced pluripotent stem cells and a native-like, high-resolution, 3-dimensionally printed scaffold, Circ. Res. 120 (8) (2017 Apr 14) 1318–1325.

[86] P. Cheng, W. Tang, H. He, Two-photon activation of endogenous store-operated calcium channels without optogenetics, in: Multiphoton Microscopy in the Biomedical Sciences XVIII 10498, 2018 Feb 23, p. 1049828 (International Society for Optics and Photonics).

[87] R.P. Briñas, T. Troxler, R.M. Hochstrasser, S.A. Vinogradov, Phosphorescent oxygen sensor with dendritic protection and two-photon absorbing antenna, J. Am. Chem. Soc. 127 (33) (2005 Aug 24) 11851–11862.

[88] I. Sencan, T.V. Esipova, M.A. Yaseen, B. Fu, D.A. Boas, S.A. Vinogradov, M. Shahidi, S. Sakadžic, Two-photon phosphorescence lifetime microscopy of retinal capillary plexus oxygenation in mice, J. Biomed. Optic. 23 (12) (2018 Dec) 126501.

[89] L.E. Sinks, E. Roussakis, S. Sakadžic, G.P. Robbins, D.A. Hammer, A. Devor, D.A. Boas, S.A. Vinogradov, Two-photon phosphorescence lifetime microscopy (2PLM) for high resolution imaging of oxygen, in: Multiphoton Microscopy in the Biomedical Sciences XI 7903, 2011 Feb 11, p. 79032A (International Society for Optics and Photonics).

[90] L.P. Cartarozzi, P. Rieder, X. Bai, A. Scheller, A.L. de Oliveira, F. Kirchhoff, In vivo two-photon imaging of motoneurons and adjacent glia in the ventral spinal cord, J. Neurosci. Methods 299 (2018 Apr 1) 8–15.

[91] A. Forli, D. Vecchia, N. Binini, F. Succol, S. Bovetti, C. Moretti, F. Nespoli, M. Mahn, C.A. Baker, M.M. Bolton, O. Yizhar, Two-photon bidirectional control and imaging of neuronal excitability with high spatial resolution in vivo, Cell Rep. 22 (11) (2018 Mar 13) 3087–3098.

[92] F.J. Ávila, A. Gambín, P. Artal, J.M. Bueno, In vivo two-photon microscopy of the human eye, Sci. Rep. 9 (1) (2019 Jul 12) 10121.

[93] W. Denk, J.H. Strickler, W.W. Webb, Two-photon laser scanning fluorescence microscopy, Science 248 (4951) (1990 Apr 6) 73–76.

[94] F. Helmchen, W. Denk, Deep tissue two-photon microscopy, Nat. Methods 2 (12) (2005 Dec) 932–940.

[95] R.S. Fischer, Y. Wu, P. Kanchanawong, H. Shroff, C.M. Waterman, Microscopy in 3D: a biologist's toolbox, Trends Cell Biol. 21 (12) (2011 Dec 1) 682–691.

[96] B.E. Urban, J. Yi, S. Chen, B. Dong, Y. Zhu, S.H. DeVries, V. Backman, H.F. Zhang, Super-resolution two-photon microscopy via scanning patterned illumination, Phys. Rev. 91 (4) (2015 Apr 7), 042703.

[97] F. Ströhl, C.F. Kaminski, Frontiers in structured illumination microscopy, Optica 3 (6) (2016 Jun 20) 667–677.

[98] P.W. Winter, A.G. York, D. Dalle Nogare, M. Ingaramo, R. Christensen, A. Chitnis, G.H. Patterson, H. Shroff, Two-photon instant structured illumination microscopy improves the depth penetration of super-resolution imaging in thick scattering samples, Optica 1 (3) (2014 Sep 20) 181–191.

[99] S.A. Skoog, P.L. Goering, R.J. Narayan, Stereolithography in tissue engineering, J. Mater. Sci. Mater. Med. 25 (3) (2014 Mar 1) 845–856.

[100] B. Husár, M. Hatzenbichler, V. Mironov, R. Liska, J. Stampfl, A. Ovsianikov, Photopolymerization-based additive manufacturing for the development of 3D porous scaffolds, Biomater. Bone Regen. (2014 Jan 1) 149–201 (Woodhead Publishing).

[101] A.K. Nguyen, R.J. Narayan, Two-photon polymerization for biological applications, Mater. Today 20 (6) (2017 Jul 1) 314–322.

[102] K. Obata, A. El-Tamer, L. Koch, U. Hinze, B.N. Chichkov, High-aspect 3D two-photon polymerization structuring with widened objective working range (WOW-2PP), Light Sci. Appl. 2 (12) (2013 Dec) e116.

[103] M. Gedvilas, J. Mikšys, J. Berzinš, V. Stankevič, G. Račiukaitis, Multi-photon absorption enhancement by dual-wavelength double-pulse laser irradiation for efficient dicing of sapphire wafers, Sci. Rep. 7 (1) (2017 Jul 12) 5218.

[104] M. Babin, D. Stramski, Light absorption by aquatic particles in the near-infrared spectral region, Limnol. Oceanogr. 47 (3) (2002 May) 911–915.

[105] C. Xu, J.B. Shear, W.W. Webb, Hyper-Rayleigh and hyper-Raman scattering background of liquid water in two-photon excited fluorescence detection, Anal. Chem. 69 (7) (1997 Apr 1) 1285–1287.

[106] M. Malinauskas, H. Gilbergs, A. Žukauskas, V. Purlys, D. Paipulas, R. Gadonas, A femtosecond laser-induced two-photon photopolymerization technique for structuring microlenses, J. Optic. 12 (3) (2010 Feb 1), 035204.

[107] H.H. Hamama, Recent advances in posterior resin composite restorations, Applications of Nanocomposite Materials in Dentistry (2019 Jan 1) 319–336 (Woodhead Publishing).

[108] A. Ovsianikov, B. Chichkov, P. Mente, N.A. Monteiro-Riviere, A. Doraiswamy, R.J. Narayan, Two photon polymerization of polymer–ceramic hybrid materials for transdermal drug delivery, Int. J. Appl. Ceram. Technol. 4 (1) (2007 Jan) 22–29.

[109] A. Doraiswamy, C. Jin, R.J. Narayan, P. Mageswaran, P. Mente, R. Modi, R. Auyeung, D.B. Chrisey, A. Ovsianikov, B. Chichkov, Two photon induced polymerization of organic–inorganic hybrid biomaterials for microstructured medical devices, Acta Biomater. 2 (3) (2006 May 1) 267–275.

[110] S. Schlie, A. Ngezahayo, A. Ovsianikov, T. Fabian, H.A. Kolb, H. Haferkamp, B.N. Chichkov, Three-dimensional cell growth on structures fabricated from ORMOCER® by two-photon polymerization technique, J. Biomater. Appl. 22 (3) (2007 Nov) 275–287.

[111] S. Amberg-Schwab, Inorganic-organic Polymers with Barrier Properties against Water Vapor, Oxygen and Migrating Monomers. Handbook of Sol-Gel Science and Technology-3. Applications of Sol-Gel Technology, Springer, 2005, pp. 455–478.

[112] J. Schwaiger, D. Collin, S. Amberg-Schwab, G. Sextl, Study on Functional Coatings for Food, Cosmetic and Pharmaceutical Packaging on the Basis of Biodegradable ORMOCER® S, 2014.

[113] A. Ovsianikov, A. Ostendorf, B.N. Chichkov, Three-dimensional photofabrication with femtosecond lasers for applications in photonics and biomedicine, Appl. Surf. Sci. 253 (15) (2007 May 30) 6599–6602.

[114] C. Schizas, D. Karalekas, Mechanical characteristics of an Ormocomp® biocompatible hybrid photopolymer, J. Mech. Behav. Biomed. Mater. 4 (1) (2011 Jan 1) 99–106.

[115] A. Marino, C. Filippeschi, G.G. Genchi, V. Mattoli, B. Mazzolai, G. Ciofani, The Osteoprint: a bioinspired two-photon polymerized 3-D structure for the enhancement of bone-like cell differentiation, Acta Biomater. 10 (10) (2014 Oct 1) 4304–4313.

[116] J. Mačiulaitis, M. Deveikytė, S. Rekštytė, M. Bratchikov, A. Darinskas, A. Šimbelytė, G. Daunoras, A. Laurinavičienė, A. Laurinavičius, R. Gudas, M. Malinauskas, Preclinical study of SZ2080 material 3D microstructured scaffolds for cartilage tissue engineering made by femtosecond direct laser writing lithography, Biofabrication 7 (1) (2015 Mar 23), 015015.

[117] J. Maciulaitis, M. Miskiniene, S. Rekštytė, M. Bratchikov, A. Darinskas, A. Simbelyte, G. Daunoras, A. Laurinaviciene, A. Laurinavicius, R. Gudas, M. Malinauskas, Osteochondral repair and electromechanical evaluation of custom 3D scaffold microstructured by direct laser writing lithography, Cartilage (2019 May 9), 1947603519847745.

[118] A. Trautmann, M. Rüth, H.D. Lemke, T. Walther, R. Hellmann, Two-photon polymerization based large scaffolds for adhesion and proliferation studies of human primary fibroblasts, Optic Laser. Technol. 106 (2018 Oct 1) 474–480.

[119] F. Guillemot, A. Souquet, S. Catros, B. Guillotin, J. Lopez, M. Faucon, B. Pippenger, R. Bareille, M. Rémy, S. Bellance, P. Chabassier, High-throughput laser printing of cells and biomaterials for tissue engineering, Acta Biomater. 6 (7) (2010 Jul 1) 2494–2500.

[120] A. Marino, J. Barsotti, G. de Vito, C. Filippeschi, B. Mazzolai, V. Piazza, M. Labardi, V. Mattoli, G. Ciofani, Two-photon lithography of 3D nanocomposite piezoelectric scaffolds for cell stimulation, ACS Appl. Mater. Interfaces 7 (46) (2015 Nov 25) 25574–25579.

[121] D.M. Zuev, E.S. Klimashina, M. Kikuchi, S. Oshima, J. Labuta, V.I. Putlyaev, P.V. Evdokimov, Y.Y. Filippov, T.V. Safronova, Mixed Ca2+/Na+ (Mg2+) polyphosphates for polymer matrix filling and their solubility, in: IOP Conference Series: Materials Science and Engineering, vol. 447, IOP Publishing, 2018 Nov, 012020, 1.

[122] A. Trautmann, B. Götzendorfer, T. Walther, R. Hellmann, Scaffolds in a shell–a new approach combining one-photon and two-photon polymerization, Optic Express 26 (23) (2018 Nov 12) 29659–29668.

[123] T. Zandrini, O. Shan, V. Parodi, G. Cerullo, M.T. Raimondi, R. Osellame, Multi-foci laser microfabrication of 3D polymeric scaffolds for stem cell expansion in regenerative medicine, Sci. Rep. 9 (1) (2019 Aug 13) 1–9.

[124] T. Stichel, B. Hecht, R. Houbertz, G. Sextl, Two-photon polymerization as method for the fabrication of large scale biomedical scaffold applications, J. Laser Micro/Nanoeng. 5 (3) (2010 Dec 1).

[125] D. Perevoznik, R. Nazir, R. Kiyan, K. Kurselis, B. Koszarna, D.T. Gryko, B.N. Chichkov, High-speed two-photon polymerization 3D printing with a microchip laser at its fundamental wavelength, Optic Express 27 (18) (2019 Sep 2) 25119–25125.

[126] B.W. Pearre, C. Michas, J.M. Tsang, T.J. Gardner, T.M. Otchy, Fast micron-scale 3D printing with a resonant-scanning two-photon microscope, Addit. Manuf. 30 (2019 Dec 1) 100887.

[127] W. Chu, Y. Tan, P. Wang, J. Xu, W. Li, J. Qi, Y. Cheng, Centimeter-height 3D printing with femtosecond laser two-photon polymerization, Adv. Mater. Technol. 3 (5) (2018 May) 1700396.

[128] G. Seniutinas, A. Weber, C. Padeste, I. Sakellari, M. Farsari, C. David, Beyond 100 nm resolution in 3D laser lithography—post processing solutions, Microelectron. Eng. 191 (2018 May 5) 25–31.

[129] X. Yu, M. Zhang, S. Lei, Multiphoton polymerization using femtosecond Bessel beam for layerless three-dimensional printing, J. Micro Nano-Manufacturing 6 (1) (2018 Mar 1), 010901.

[130] G.S. Sokolovskii, V.V. Dudelev, S.N. Losev, K.K. Soboleva, A.G. Deryagin, K.A. Fedorova, V.I. Kuchinskii, W. Sibbett, E.U. Rafailov, Bessel beams from semiconductor light sources, Prog. Quant. Electron. 38 (4) (2014 Jul 1) 157–188.

[131] S.K. Saha, D. Wang, V.H. Nguyen, Y. Chang, J.S. Oakdale, S.C. Chen, Scalable submicrometer additive manufacturing, Science 366 (6461) (2019 Oct 4) 105–109.

[132] D.H. Froula, D. Turnbull, A.S. Davies, T.J. Kessler, D. Haberberger, J.P. Palastro, S.W. Bahk, I.A. Begishev, R. Boni, S. Bucht, J. Katz, Spatiotemporal control of laser intensity, Nat. Photon. 12 (5) (2018 May) 262.

[133] T. Stichel, B. Hecht, R. Houbertz, G. Sextl, Compensation of spherical aberration influences for two-photon polymerization patterning of large 3D scaffolds, Appl. Phys. A 121 (1) (2015 Oct 1) 187–191.

[134] F. Korte, J. Serbin, J. Koch, A. Egbert, C. Fallnich, A. Ostendorf, B.N. Chichkov, Towards nanostructuring with femtosecond laser pulses, Appl. Phys. A 77 (2) (2003 Jul 1) 229–235.

[135] R. Wollhofen, J. Katzmann, C. Hrelescu, J. Jacak, T.A. Klar, 120 nm resolution and 55 nm structure size in STED-lithography, Optic Express 21 (9) (2013 May 6) 10831–10840.

[136] T.A. Klar, R. Wollhofen, J. Jacak, Sub-Abbe resolution: from STED microscopy to STED lithography, Phys. Scripta 2014 (T162) (2014 Sep 19), 014049.

[137] N. Kedia, Z. Liu, R.D. Sochol, J. Tam, D.X. Hammer, A. Agrawal, 3-D printed photoreceptor phantoms for evaluating lateral resolution of adaptive optics imaging systems, Optic. Lett. 44 (7) (2019 Apr 1) 1825–1828.

[138] L. Zheng, K. Kurselis, A. El-Tamer, U. Hinze, C. Reinhardt, L. Overmeyer, B. Chichkov, Nanofabrication of high-resolution periodic structures with a gap size below 100 nm by two-photon polymerization, Nanoscale Res. Lett. 14 (1) (2019 Dec) 1–9.

[139] S.H. Park, T.W. Lim, D.Y. Yang, R.H. Kim, K.S. Lee, Improvement of spatial resolution in nano-stereolithography using radical quencher, Macromol. Res. 14 (5) (2006 Oct 1) 559–564.

[140] Y. Bougdid, I. Maouli, A. Rahmouni, K. Mochizuki, I. Bennani, M. Halim, Z. Sekkat, Systematic λ/21 resolution achieved in nanofabrication by two-photon-absorption induced polymerization, J. Micromech. Microeng. 29 (3) (2019 Feb 1), 035018.

[141] S. Wang, Y. Yu, H. Liu, K.T. Lim, B.M. Srinivasan, Y.W. Zhang, J.K. Yang, Sub-10-nm suspended nano-web formation by direct laser writing, Nano Futures 2 (2) (2018 May 21), 025006.

[142] M.P. Stocker, L. Li, R.R. Gattass, J.T. Fourkas, Multiphoton photoresists giving nanoscale resolution that is inversely dependent on exposure time, Nat. Chem. 3 (3) (2011 Mar) 223.

[143] A. Ostendorf, B.N. Chichkov, Two-photon polymerization: a new approach to micromachining, Photon. Spectra. 40 (10) (2006 Oct 1) 72.

[144] W. Zhou, S.M. Kuebler, K.L. Braun, T. Yu, J.K. Cammack, C.K. Ober, J.W. Perry, S.R. Marder, An efficient two-photon-generated photoacid applied to positive-tone 3D microfabrication, Science 296 (5570) (2002 May 10) 1106–1109.

[145] N. Tsutsumi, A. Fukuda, R. Nakamura, K. Kinashi, W. Sakai, Fabrication of three-dimensional microstructures in positive photoresist through two-photon direct laser writing, Appl. Phys. A 123 (8) (2017 Aug 1) 553.

[146] H.Z. Cao, M.L. Zheng, X.Z. Dong, F. Jin, Z.S. Zhao, X.M. Duan, Two-photon nanolithography of positive photoresist thin film with ultrafast laser direct writing, Appl. Phys. Lett. 102 (20) (2013 May 20) 201108.

[147] Zyla G, Aumann A, Ksouri SI, Gurevich EL, Ostendorf A. Precise Structuring by 2-photon Absorption in Positive Photoresist Materials.

[148] J.H. Lake, S.D. Cambron, K.M. Walsh, S. McNamara, Maskless grayscale lithography using a positive-tone photodefinable polyimide for MEMS applications, J. Microelectromech. Syst. 20 (6) (2011 Oct 3) 1483–1488.

[149] T. Yu, C.K. Ober, S.M. Kuebler, W. Zhou, S.R. Marder, J.W. Perry, Chemically amplified positive resists for two-photon three-dimensional microfabrication, Adv. Mater. 15 (6) (2003 Mar 17) 517–521.

[150] A. Ovsianikov, M. Malinauskas, S. Schlie, B. Chichkov, S. Gittard, R. Narayan, M. Löbler, K. Sternberg, K.P. Schmitz, A. Haverich, Three-dimensional laser micro- and nano-structuring of acrylated poly (ethylene glycol) materials and evaluation of their cytoxicity for tissue engineering applications, Acta Biomater. 7 (3) (2011 Mar 1) 967–974.

[151] G. Merkininkaitė, D. Gailevičius, S. Šakirzanovas, L. Jonušauskas, Polymers for regenerative medicine structures made via multiphoton 3D lithography, Int. J. Polym. Sci. 2019 (2019).

[152] H. Jiang, C. Tian, L. Zhang, Z. Cheng, X. Zhu, Facile and highly efficient "living" radical polymerization of hydrophilic vinyl monomers in water, RSC Adv. 4 (94) (2014) 52430–52437.

[153] Z. Li, J. Torgersen, A. Ajami, S. Mühleder, X. Qin, W. Husinsky, W. Holnthoner, A. Ovsianikov, J. Stampfl, R. Liska, Initiation efficiency and cytotoxicity of novel water-soluble two-photon photoinitiators for direct 3D microfabrication of hydrogels, RSC Adv. 3 (36) (2013) 15939–15946.

[154] M. Tromayer, P. Gruber, M. Markovic, A. Rosspeintner, E. Vauthey, H. Redl, A. Ovsianikov, R. Liska, A biocompatible macromolecular two-photon initiator based on hyaluronan, Polym. Chem. 8 (2) (2017) 451–460.

[155] X. Huang, X. Wang, Y. Zhao, Study on a series of water-soluble photoinitiators for fabrication of 3D hydrogels by two-photon polymerization, Dyes Pigments 141 (2017 Jun 1) 413–419.

[156] A.A. Pawar, G. Saada, I. Cooperstein, L. Larush, J.A. Jackman, S.R. Tabaei, N.J. Cho, S. Magdassi, High-performance 3D printing of hydrogels by water-dispersible photoinitiator nanoparticles, Sci. Adv. 2 (4) (2016 Apr 1), e1501381.

[157] O. Kufelt, A. El-Tamer, C. Sehring, M. Meißner, S. Schlie-Wolter, B.N. Chichkov, Water-soluble photopolymerizable chitosan hydrogels for biofabrication via two-photon polymerization, Acta Biomater. 18 (2015 May 1) 186–195.

[158] C. Loebel, N. Broguiere, M. Alini, M. Zenobi-Wong, D. Eglin, Microfabrication of photo-cross-linked hyaluronan hydrogels by single-and two-photon tyramine oxidation, Biomacromolecules 16 (9) (2015 Sep 14) 2624–2630.

[159] L. Luo Zheng, V. Vanchinathan, R. Dalal, J. Noolandi, D.J. Waters, L. Hartmann, J.R. Cochran, C.W. Frank, C.Q. Yu, C.N. Ta, Biocompatibility of poly (ethylene glycol) and poly (acrylic acid) interpenetrating network hydrogel by intrastromal implantation in rabbit cornea, J. Biomed. Mater. Res. 103 (10) (2015 Oct) 3157–3165.

[160] L. Jiang, W. Xiong, Y. Zhou, Y. Liu, X. Huang, D. Li, T. Baldacchini, L. Jiang, Y. Lu, Performance comparison of acrylic and thiol-acrylic resins in two-photon polymerization, Optic Express 24 (12) (2016 Jun 13) 13687–13701.

[161] T. Zandrini, N. Liaros, L.J. Jiang, Y.F. Lu, J.T. Fourkas, R. Osellame, T. Baldacchini, Effect of the resin viscosity on the writing properties of two-photon polymerization, Opt. Mater. Express 9 (6) (2019 Jun 1) 2601–2616.

[162] K. Yue, G. Trujillo-de Santiago, M.M. Alvarez, A. Tamayol, N. Annabi, A. Khademhosseini, Synthesis, properties, and biomedical applications of gelatin methacryloyl (GelMA) hydrogels, Biomaterials 73 (2015 Dec 1) 254–271.

[163] A. Ovsianikov, A. Deiwick, S. Van Vlierberghe, M. Pflaum, M. Wilhelmi, P. Dubruel, B. Chichkov, Laser fabrication of 3D gelatin scaffolds for the generation of bioartificial tissues, Materials 4 (1) (2011 Jan) 288–299.
[164] S. Bertlein, G. Brown, K.S. Lim, T. Jungst, T. Boeck, T. Blunk, J. Tessmar, G.J. Hooper, T.B. Woodfield, J. Groll, Thiol–ene clickable gelatin: a platform bioink for multiple 3D biofabrication technologies, Adv. Mater. 29 (44) (2017 Nov) 1703404.
[165] K.S. Lim, B.S. Schon, N.V. Mekhileri, G.C. Brown, C.M. Chia, S. Prabakar, G.J. Hooper, T.B. Woodfield, New visible-light photoinitiating system for improved print fidelity in gelatin-based bioinks, ACS Biomater. Sci. Eng. 2 (10) (2016 Oct 10) 1752–1762.
[166] H. Shih, C.C. Lin, Visible-light-mediated thiol-Ene hydrogelation using eosin-Y as the only photoinitiator, Macromol. Rapid Commun. 34 (3) (2013 Feb 12) 269–273.
[167] G.J. Graulus, A. Mignon, S. Van Vlierberghe, H. Declercq, K. Fehér, M. Cornelissen, J.C. Martins, P. Dubruel, Cross-linkable alginate-graft-gelatin copolymers for tissue engineering applications, Eur. Polym. J. 72 (2015 Nov 1) 494–506.
[168] M. Tromayer, A. Dobos, P. Gruber, A. Ajami, R. Dedic, A. Ovsianikov, R. Liska, A biocompatible diazosulfonate initiator for direct encapsulation of human stem cells via two-photon polymerization, Polym. Chem. 9 (22) (2018) 3108–3117.
[169] J. Van Hoorick, P. Gruber, M. Markovic, M. Tromayer, J. Van Erps, H. Thienpont, R. Liska, A. Ovsianikov, P. Dubruel, S. Van Vlierberghe, Cross-linkable gelatins with superior mechanical properties through carboxylic acid modification: increasing the two-photon polymerization potential, Biomacromolecules 18 (10) (2017 Oct 9) 3260–3272.
[170] J. Van Hoorick, P. Gruber, M. Markovic, M. Rollot, G.J. Graulus, M. Vagenende, M. Tromayer, J. Van Erps, H. Thienpont, J.C. Martins, S. Baudis, Highly reactive thiol-norbornene photo-click hydrogels: toward improved processability, Macromol. Rapid Commun. 39 (14) (2018 Jul) 1800181.
[171] A. Koroleva, A. Deiwick, A. Nguyen, S. Schlie-Wolter, R. Narayan, P. Timashev, V. Popov, V. Bagratashvili, B. Chichkov, Osteogenic differentiation of human mesenchymal stem cells in 3-D Zr-Si organic-inorganic scaffolds produced by two-photon polymerization technique, PloS One 10 (2) (2015).
[172] D.W. Hutmacher, Scaffolds in tissue engineering bone and cartilage, Biomaterials 21 (24) (2000 Dec 15) 2529–2543.
[173] F. Claeyssens, E.A. Hasan, A. Gaidukeviciute, D.S. Achilleos, A. Ranella, C. Reinhardt, A. Ovsianikov, X. Shizhou, C. Fotakis, M. Vamvakaki, B.N. Chichkov, Three-dimensional biodegradable structures fabricated by two-photon polymerization, Langmuir 25 (5) (2009 Mar 3) 3219–3223.
[174] A. Shpichka, A. Koroleva, D. Kuznetsova, V. Burdukovskii, B. Chichkov, V. Bagratashvili, P. Timashev, Two-photon polymerization in tissue engineering, in: Polymer and Photonic Materials towards Biomedical Breakthroughs, Springer, Cham, 2018, pp. 71–98.
[175] P. Timashev, D. Kuznetsova, A. Koroleva, N. Prodanets, A. Deiwick, Y. Piskun, K. Bardakova, N. Dzhoyashvili, S. Kostjuk, E. Zagaynova, Y. Rochev, Novel biodegradable star-shaped polylactide scaffolds for bone regeneration fabricated by two-photon polymerization, Nanomedicine 11 (9) (2016 May) 1041–1053.
[176] A. Ovsianikov, M. Gruene, M. Pflaum, L. Koch, F. Maiorana, M. Wilhelmi, A. Haverich, B. Chichkov, Laser printing of cells into 3D scaffolds, Biofabrication 2 (1) (2010 Mar 10), 014104.
[177] M. Elsayed, A. Kothandaraman, M. Edirisinghe, J. Huang, Porous polymeric films from microbubbles generated using a T-junction microfluidic device, Langmuir 32 (50) (2016 Dec 20) 13377–13385.